Supporting Information

for

Snowflake-Like Cu_2O-Pt Nanocluster Mediated Fenton Photothermal and Chemodynamic for Antibiotic Wound Healing Therapy

En Li[a, b#], Qi Han[b#], Ting Chen[c], Si Cheng[b], Jinghua Li[a*]

[a] School of Medical Technology and Engineering, Henan University of Science and Technology, Luoyang 471000, China

[b] Xianning Central Hospital, The First Affiliated Hospital of Hubei University of Science and Technology, Xianning 437000, China

[c] Clinical Medicine College of Hubei University of Science and Technology，Xianning 437100,China

[#] These authors contributed equally to this work.

*Corresponding author:Jinghua Li

College of Medical Technology and Engineering, Henan University of Science and Technology, Luoyang 471000, China

Tel: +86-379-64819930

E-**mail**: anubiss1860@163.com

Experimental section

Characterization

The morphology and chemical elemental composition of the synthesized HCPNLs were characterized using scanning electron microscopy (SEM) (JEOL JSM-7800F, Japan), transmission electron microscopy (TEM), and high-resolution transmission electron microscopy (HR-TEM) (FEI Tecnai G2 F30, USA). The crystal structure and morphological details of the samples were assessed through X-ray diffractometry (XRD) (D8-Advance, Cu Kα, Germany). The electron binding energy and surface chemistry of the samples were analyzed using X-ray photoelectron spectroscopy (XPS) (PHIX-tool, ULVAC, Japan). Infrared measurements were conducted with a TP5 handheld infrared thermometer (Hikvision, China) to obtain thermograms and assess temperature variations. The concentration of organic dyes in solution was quantified using a UV-Vis spectrophotometer (Nanodrop One, Thermo Fisher Scientific, USA). Bacterial and cellular morphologies were examined via scanning electron microscopy (SEM，Germany) and confocal laser scanning microscopy (CLSM，Germany).

Photothermal conversion efficiency (η) of HCPNLs

According to Li's report(Li et al., 2022), the photothermal conversion efficiency (η) is

calculated by the following equation:

$$\eta = \frac{hA(\Delta T_{max} - \Delta T_{max,H_2O})}{I(1\text{-}10^{-A_\lambda})}$$

Where h is the heat transfer coefficient, A is the surface area of the vessel, and

ΔT_{max} is is the temperature change of the HCPNLs solution at the maximum steady state temperature under NIR light irradiation. $\Delta T_{max,H_2O}$ is the temperature change of water under the same conditions. I is the power density of the NIR laser. A_λ is the light absorption value of HCPNLs at 808 nm.

$$\tau_S = \frac{\sum_i m_i c_{p,i}}{hA}$$

The equation can be simplified since the mass of HCPNLs is much lower than that of water:

$$\tau_S = \frac{m_{H_2O} c_{H_2O}}{hA}$$

$m_{H_2O}$is the mass of water, C_{H_2O} is the specific heat capacity of water (4.2 $J \bullet g^{-1} \bullet C^{-1}$), and τ_s is the time constant, calculated by Eq:

$$\tau_S = \frac{t}{-\ln\theta}$$

$$\theta = \frac{T_{surr} - T}{T_{surr} - T_{max}}$$

t is the real time cooling time and T is the real time temperature of t. T_{surr} is the ambient temperature. T_{max} is the maximum stabilisation temperature of the solution.

A

B

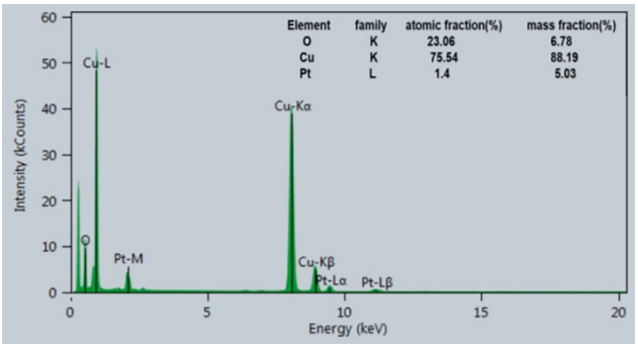

Fig. S1 (A) HAADF of HCPNLs. (B) EDX analysis of HCPNLs.

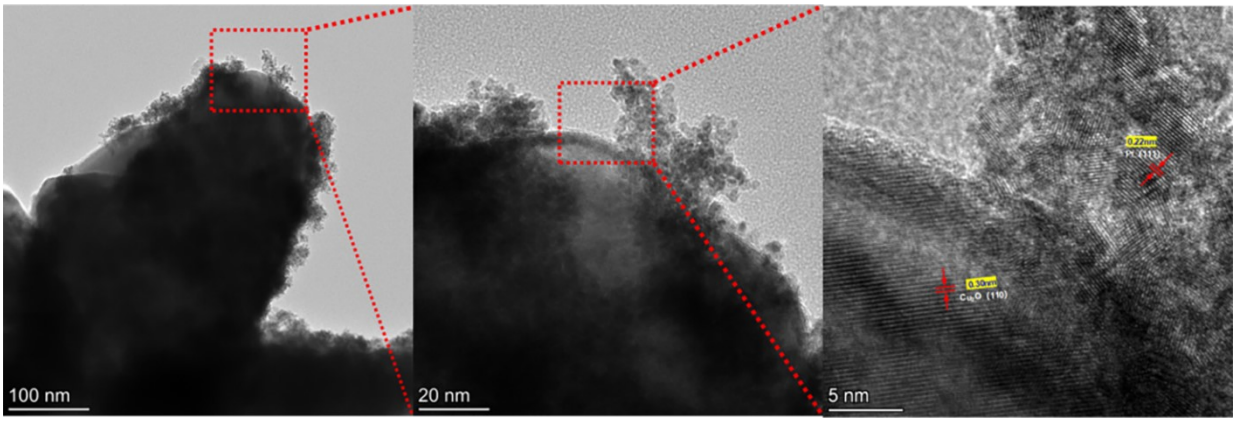

Fig. S2 HRTEM of HCPNLs and the lattice fringes of Cu_2O and Pt.

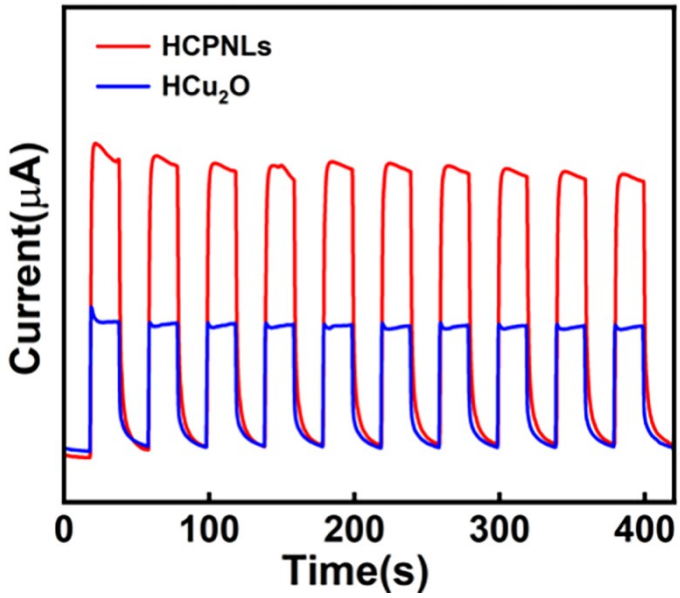

Fig. S3 Photoelectric current measurements of HCu_2O and HCPNLs.

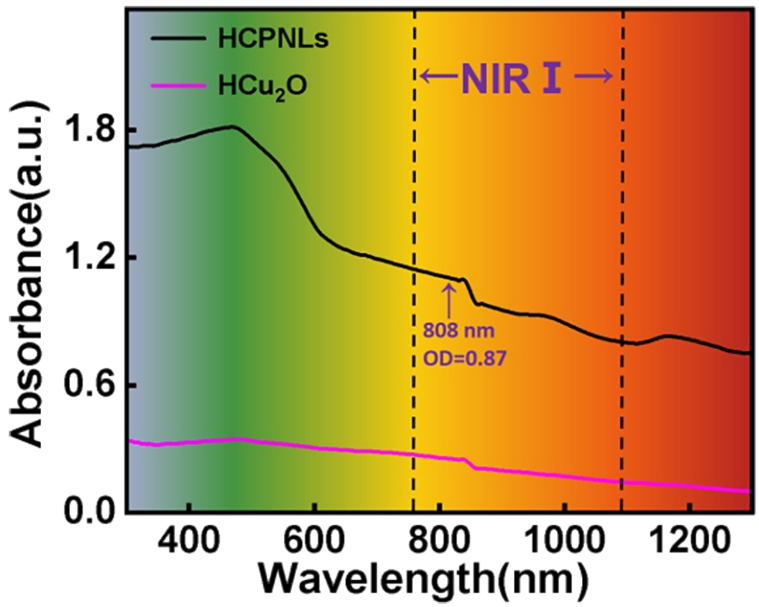

Fig. S4 UV-Vis absorbance spectrum of HCPNLs.

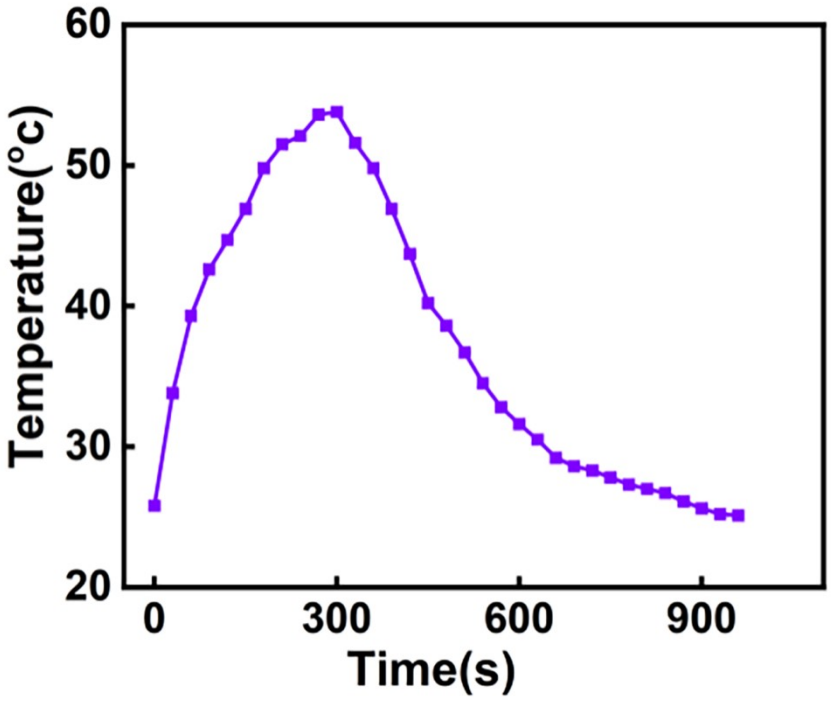

Fig. S5 Heating and cooling curves of HCPNLs under laser irradiation (NIR:808 nm, 2.0 w•cm^{-2}).

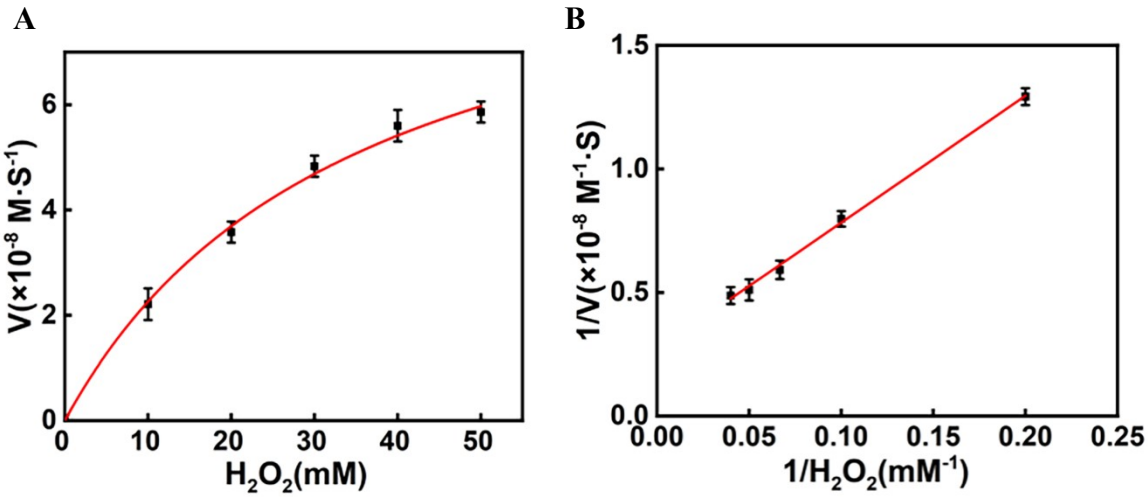

Fig. S6 Michaelis-Menten kinetic (A) and Lineweaver-Burk plotting (B) for HCPNLs with TMB and H_2O_2 .

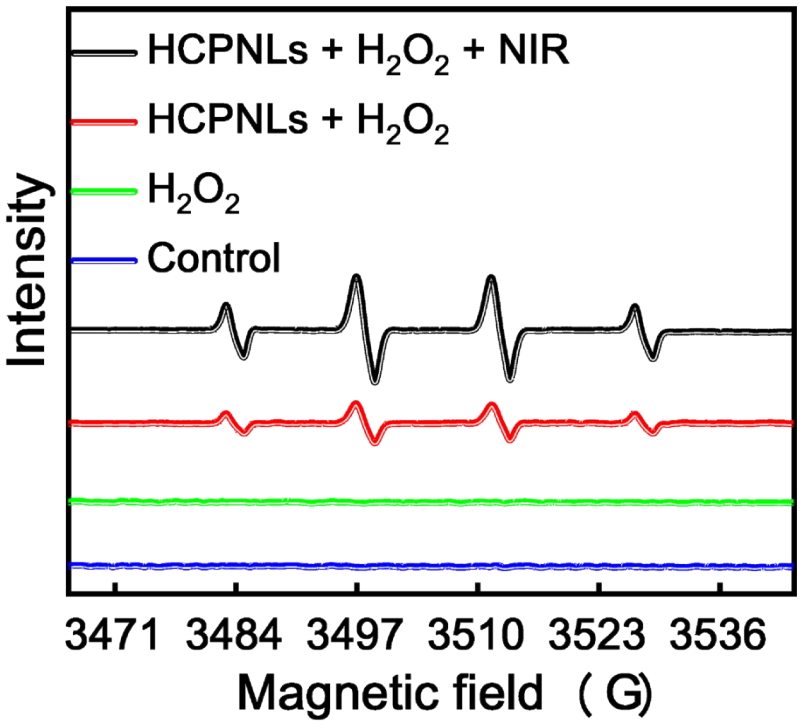

Fig. S7 EPR spectra under different reaction conditions.

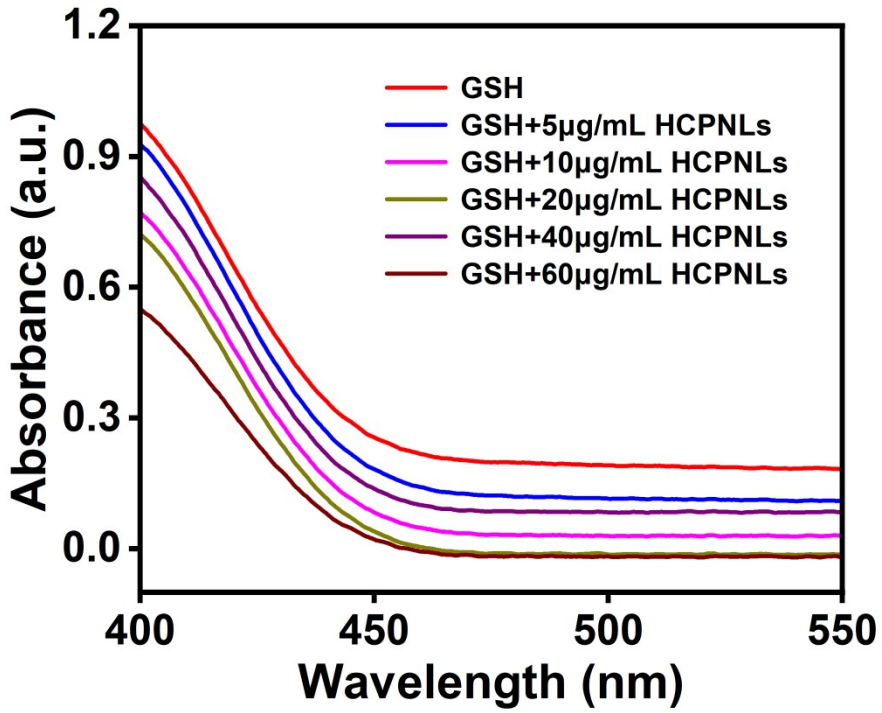

Fig. S8 GSH consumption caused by different concentrations of HCPNLs (5, 10, 20, 40 and 60 μg/mL).

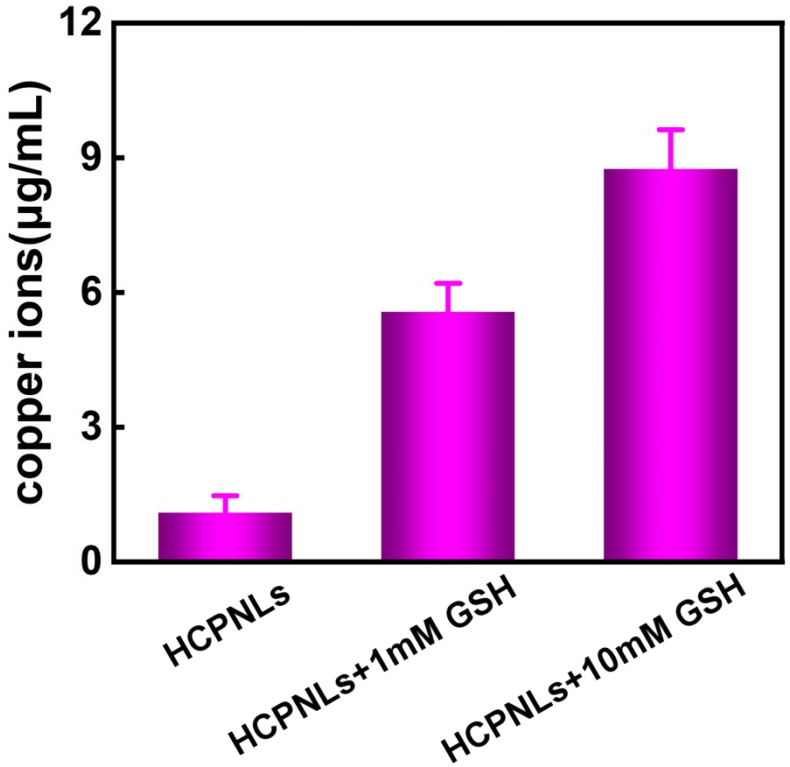

Fig. S9 The copper ion release from HCPNLs solution was measured by ICP-OES HCPNLs (60 μg/mL) treated with different concentrations of GSH for 4 h.

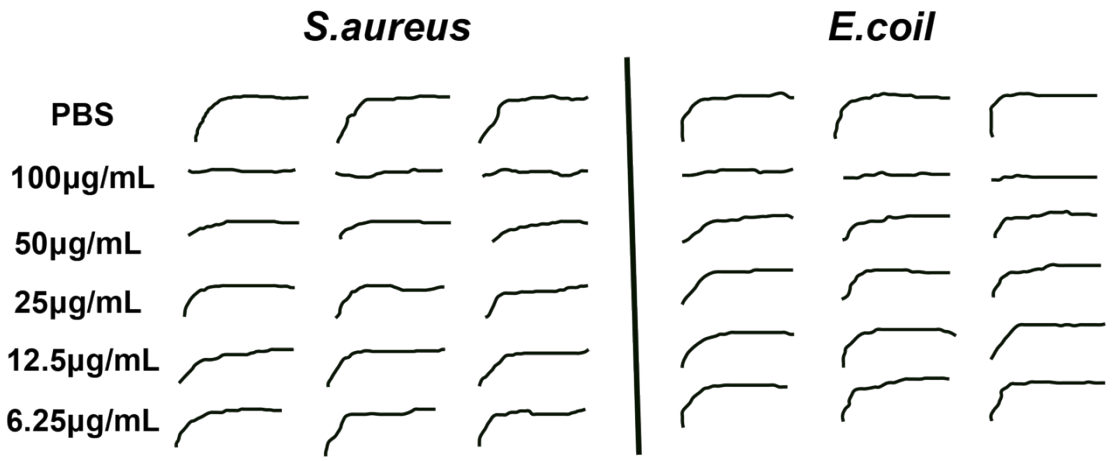

Fig. S10 Representative growth curves of bacteria after treatment with different concentrations of material.

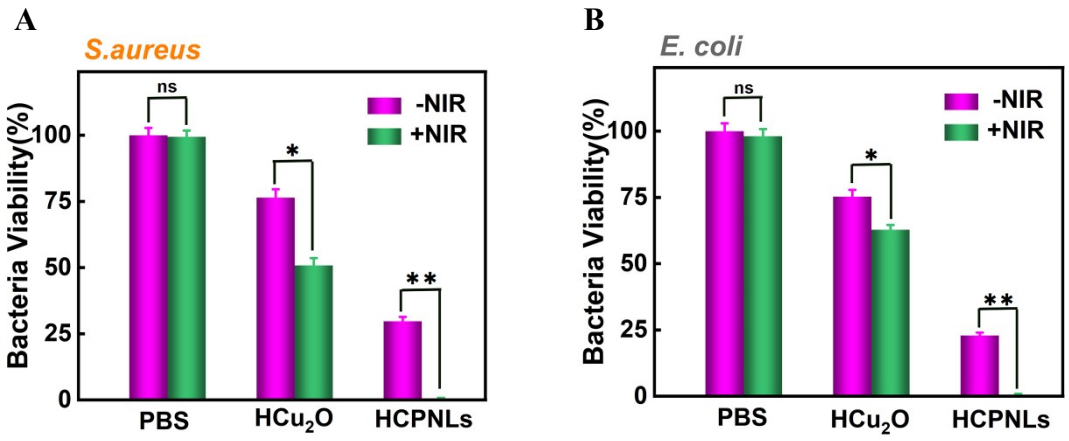

Fig. S11 In vitro antimicrobial assay of PBS, HCu_2O, and HCPNLs (NIR: 2.0 w•cm^{-2}, H_2O_2: 1 mM, Concentration of catalyst: 60 μg•mL^{-1}). (mean ± sem, n = 3, *p < 0.05, **p < 0.01, ***p < 0.001).

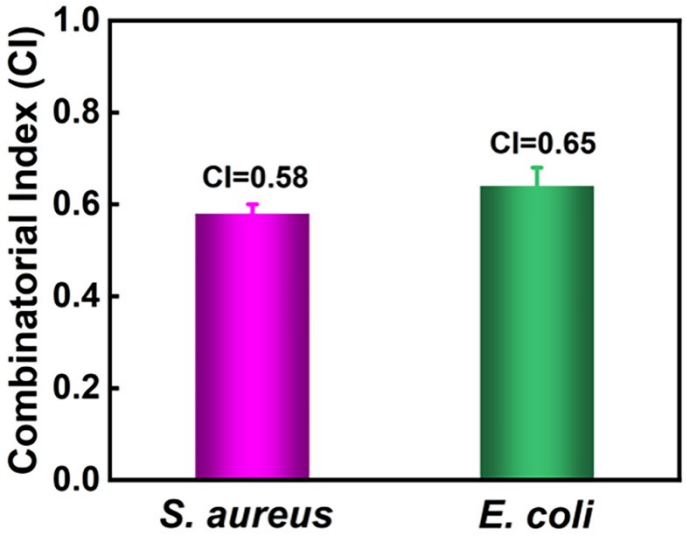

Fig. S12 HCPNLs in vitro antimicrobial Combination index.

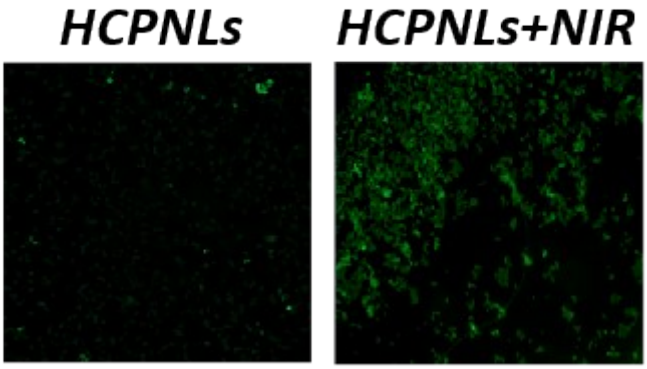

Fig. S13 Confocal images of ROS levels after different treatments.

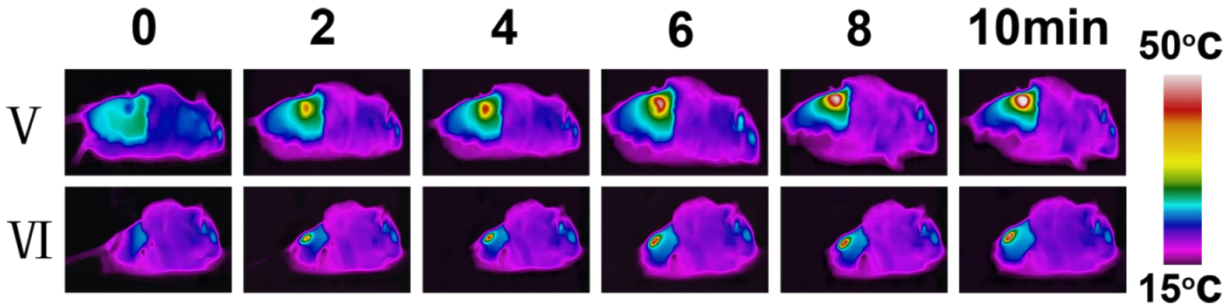

Fig. S14 Infrared thermogram of rats irradiated with a near-infrared laser. (NIR:808 nm, 2.0 w•cm^{-2})

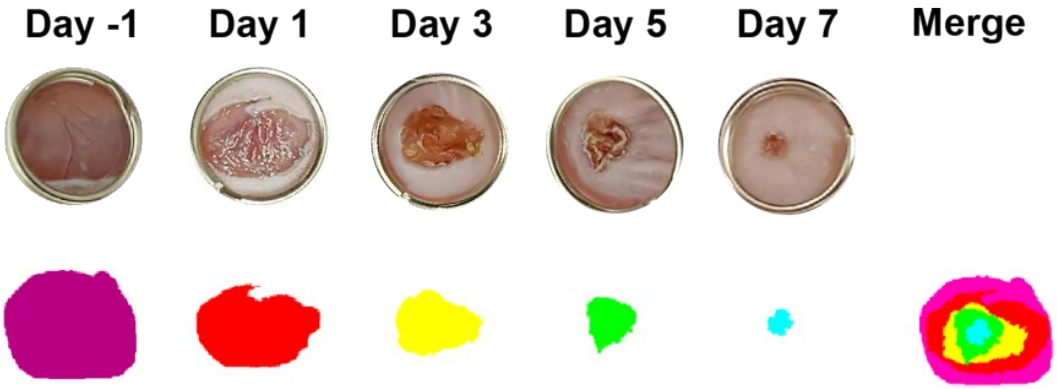

Fig. S15 Pictures of healed wounds and corresponding healing marks in the penicillin grou of bacterial colonisation.

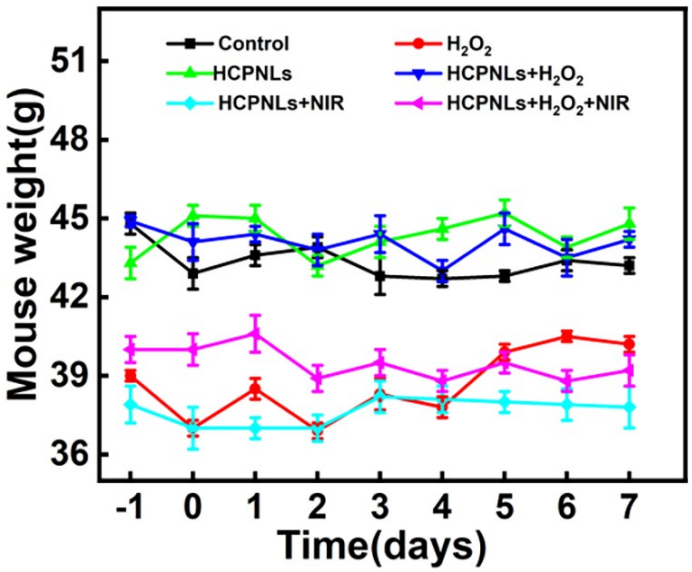

Fig. S16 Changes in body weight of mice in different groups.

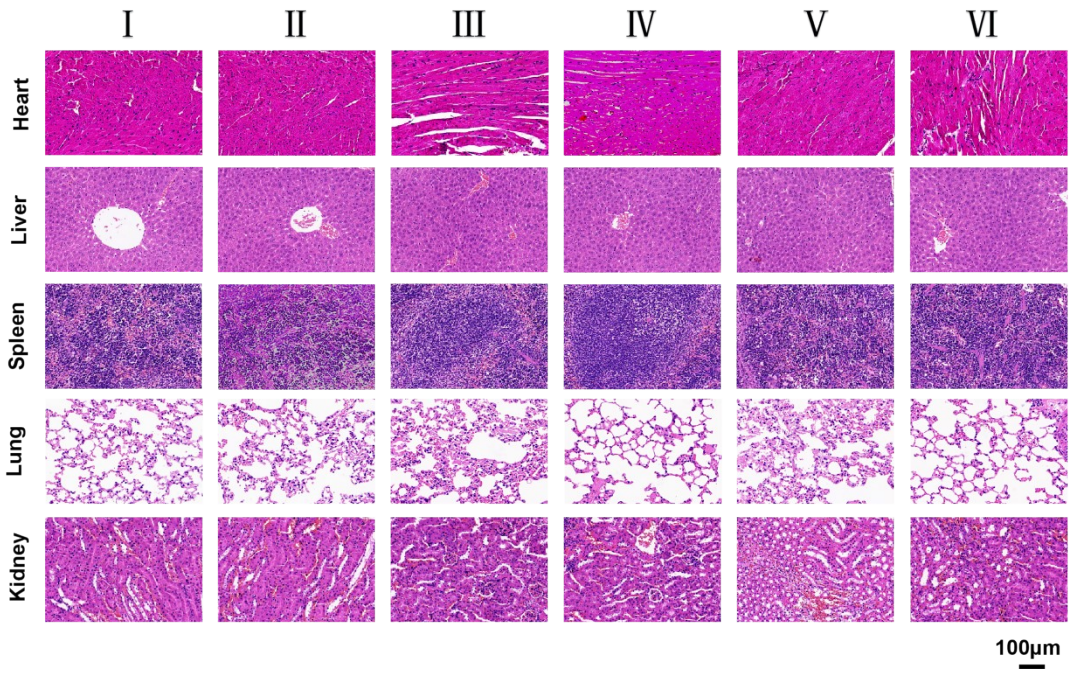

Fig. S17 H&E staining of major organs (heart, liver, spleen, lungs and kidneys) of mice in different treatment groups.

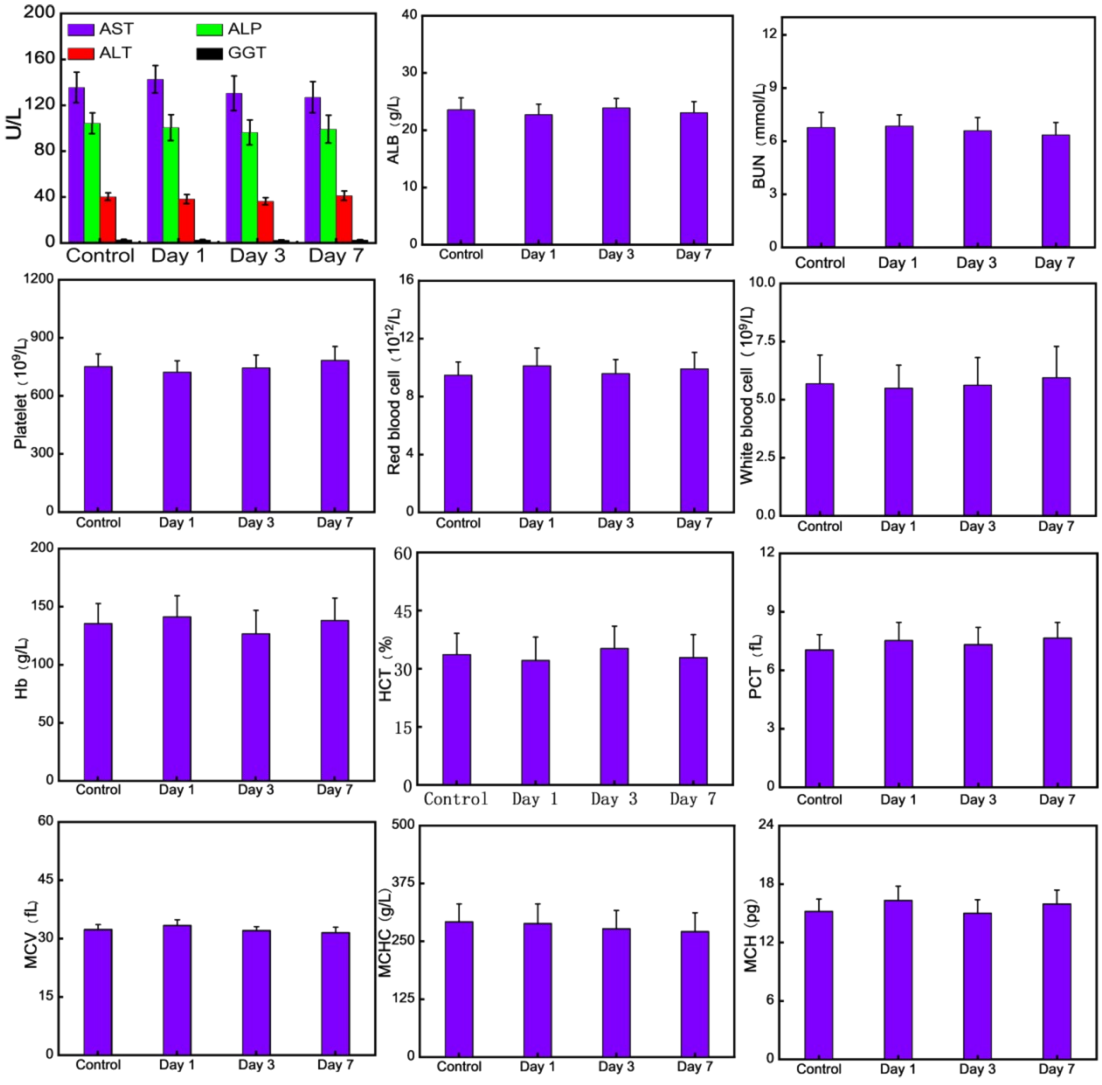

Fig. S18 Blood routine indicators of mice upon different treatment for 7 days.

References

Li, X., S. Luo, Y. Chen, et al., 2022. Facile One-Pot Synthesis of Meteor Hammer-like Au-MnOx Nanozymes with Spiky Surface for NIR-II Light-Enhanced Bacterial Elimination. Chemistry of Materials. 34, 9876-9891. https://doi.org/10.1021/acs.chemmater.2c01775